

Tạp chí

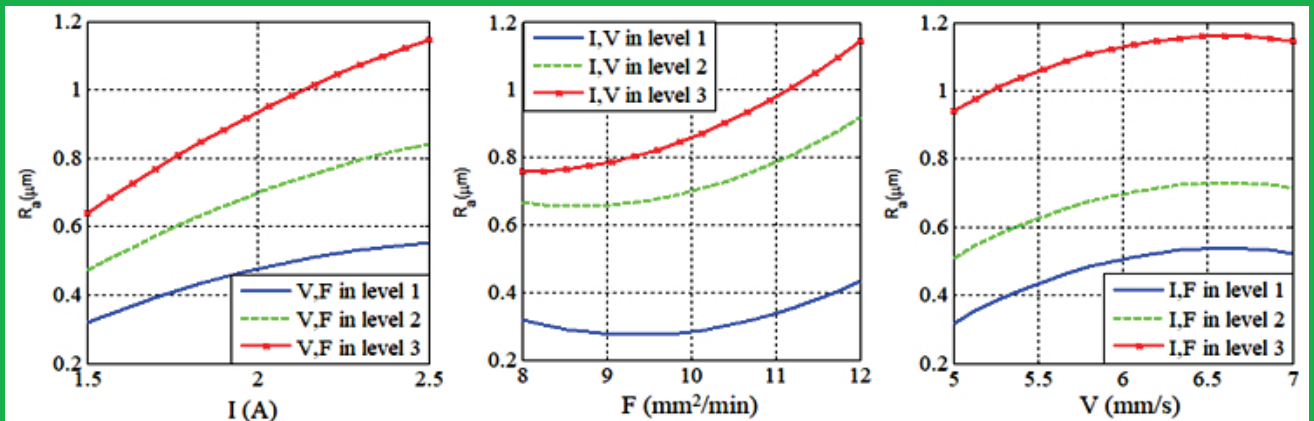
KHOA HỌC VÀ

CÔNG NGHỆ ỨNG DỤNG

JOURNAL OF APPLIED SCIENCE AND TECHNOLOGY

Số 48

Tháng 12/2025



MỤC LỤC

STT		Trang
1.	Nguyen Hong Phong, Van- The Tran, Thuan – Hoang Minh, and Vu Duc Phuc STATISTICAL MODELING AND OPTIMIZATION OF SURFACE ROUGHNESS IN WIRE EDM OF NONCIRCULAR GEARS MADE OF SKD11 STEEL Mô hình hóa thống kê và tối ưu hóa độ nhám bề mặt trong gia công EDM các bánh răng không tròn làm từ thép SKD11	5
2.	Trong-Tung Dam, Thi-Quy Vu, Xuan-Truong Vu, Dinh-Quan Doan VELOCITY-DEPENDENT DEFORMATION MECHANISM OF FENICRCOTI HIGH-ENTROPY ALLOY UNDER VIBRATION-ASSISTED MACHINING Cơ chế biến dạng phụ thuộc vận tốc của hợp kim entropy cao FeNiCrCoTi trong quá trình gia công hỗ trợ rung động	12
3.	Van-Duong Vuong, Minh-Thuan Hoang CUTTER CORRECTION METHOD FOR IMPROVING THE ACCURACY OF MANUFACTURED SCREW ROTOR BY END MILLING CUTTER Phương pháp hiệu chỉnh dụng cụ cắt để nâng cao độ chính xác gia công rotor trục vít bằng dao phay ngón	19
4.	Trong-Linh Nguyen, Anh-Vu Pham, Van-Thoai Nguyen ATOMISTIC INSIGHTS INTO Al/Al EXPLOSIVE WELDING: A MOLECULAR DYNAMICS STUDY OF INTERFACIAL BONDING AND DIFFUSION MECHANISMS Nghiên cứu ở cấp nguyên tử quá trình hàn nổ Al/Al bằng mô phỏng động lực học phân tử về cơ chế liên kết và khuếch tán tại giao diện	25
5.	Anh-Vu Pham, Trong-Linh Nguyen INDENTATION SIZE EFFECT ON THE DEFORMATION BEHAVIOR OF Ta-Cu AMORPHOUS THIN FILMS Ảnh hưởng của kích thước dụng cụ đến hành vi biến dạng của màng mỏng vô định hình Ta-Cu	32
6.	Nguyễn Thị Vân Anh, Nguyễn Hữu Cường, Đào Văn Đã, Đỗ Thành Hiếu NGHIÊN CỨU MÔ PHỎNG HỆ THỐNG QUANG ĐIỆN BA PHA NỐI LƯỚI SỬ DỤNG KỸ THUẬT ĐIỀU CHẾ SVPWM CHO NGHỊCH LƯU Simulation Study of A Three-Phase Grid-Connected Photovoltaic System using SVPWM Technique for The Inverter	38
7.	Giànn Thị Thu Hường, Cao Thị Hoài Thủy ĐÁNH GIÁ MỘT SỐ TÍNH CHẤT CƠ LÝ CỦA VẢI DỆT KIM ĐAN DỌC SỬ DỤNG SỢI POLYESTER TÁI CHẾ Evaluation of Some Mechanical Properties of Warp-Knitted Fabrics using Recycled Polyester Yarn	45
8.	Hà Ngọc Tuấn, Phạm Thị Ánh Hương, Trần Thị Thu Huyền, Ngô Thị Lan Anh SMOTE-ENSEMBLE: TỔNG QUAN KỸ THUẬT CÂN BẰNG DỮ LIỆU VÀ MÔ HÌNH HỌC MÁY KẾT HỢP TRONG DỰ ĐOÁN SỚM BIẾN CHỨNG VỔNG MẠC ĐÁI THÁO ĐƯỜNG Smote-Ensemble: A Review of Data-Balancing Techniques and Hybrid Machine Learning Models for Early Prediction of Diabetic Retinopathy Complications	51

9. **Nguyễn Đỗ Khải Hoàn, Trần Đỗ Thu Hà, Lưu Hoàng Minh, Nguyễn Xuân Mong, Nguyễn Văn Đạt, Trương Quốc Huy, Nguyễn Thanh Bình** 58
MỘT PHƯƠNG PHÁP TIẾP CẬN HIỆU QUẢ CHO BÀI TOÁN PHÁT HIỆN VẬT THỂ BAY TRÊN KHÔNG TẦM THẤP
An Effective Approach for Low-Altitude Aerial Object Detection
10. **Bui-Van HAI, Le-Duc HIEU, Nguyen-Phi TRUONG, Lam-Quang VINH, Khong-Van Nguyen** 62
THE IMPACT OF CERTAIN WORKING PARAMETERS ON THE DRILLING PROCESS OF PERCUSSIVE-ROTARY DRILLING
Ảnh hưởng của một số thông số làm việc đến quá trình khoan xoay đập
11. **Pham Thi Trang, Do Phuc Huong** 68
USING ROLE-PLAYING ACTIVITIES TO ENHANCE SPEAKING SKILLS OF SECOND-YEAR NON-ENGLISH MAJOR STUDENTS: AN ACTION RESEARCH AT A UNIVERSITY IN HUNG YEN
Sử dụng hoạt động nhập vai nhằm nâng cao kỹ năng nói cho sinh viên không chuyên ngữ năm thứ hai: nghiên cứu hành động tại một trường đại học ở Hưng Yên
12. **Nguyễn Anh Hải** 75
NGHIÊN CỨU VÀ CHẾ TẠO MẪU ROBOT TỰ HÀNH HỖ TRỢ CÔNG TÁC ĐÀO TẠO VỚI CHỨC NĂNG NHẬN DIỆN VÀ ĐỐI THOẠI THÔNG MINH
Research and Development of an Autonomous Mobile Robot for Educational Support with Intelligent Recognition and Dialogue Functions



INDENTATION SIZE EFFECT ON THE DEFORMATION BEHAVIOR OF Ta-Cu AMORPHOUS THIN FILMS

Anh-Vu Pham*, Trong-Linh Nguyen

Hung Yen University of Technology and Education

* Corresponding author: phamanhvu@utehy.edu.vn

Received: 10/10/2025

Revised: 17/11/2025

Accepted for publication: 18/12/2025

Abstract:

Molecular dynamics simulations were conducted to investigate the deformation characteristics of Ta₄₀Cu₆₀ amorphous coatings under nanoindentation. This study provides insights into the influence of indenter size on the deformation mechanisms at the Ta₄₀Cu₆₀ amorphous coating/Cu substrate interface. The results reveal that both the maximum indentation force and the extent of the plastic deformation region increase with increasing indenter diameter.

Keywords: Coatings, Deformation, Molecular dynamics.

1. Introduction

Metallic glasses have attracted considerable attention owing to their unique combination of high strength, excellent corrosion resistance, and superior hardness, which enable applications in magnetic devices, precision molds, and electronic components [1,2]. Previous studies have demonstrated that atomic bonding structures strongly influence the elastic modulus and strength of amorphous alloys [3,4]. In particular, Ta–Cu alloys exhibit promising mechanical properties, including high impact resistance, strength, and electrical conductivity [5,6]. Among amorphous thin films, TaCu coatings have emerged as highly promising candidates due to their outstanding mechanical stability and wear resistance [7,8]. Numerous experimental studies have investigated their microstructure, hardness, and interfacial behavior under various compositions and processing conditions [9]. However, direct experimental observation of nanoscale deformation mechanisms remains challenging.

Molecular dynamics (MD) simulations provide an effective approach for investigating atomic-scale mechanisms governing deformation and failure in metallic glasses and coatings [10,11]. This method has been widely employed to explore thin-film growth, mechanical response, and defect evolution in amorphous materials [12,13]. In this study, Ta₄₀Cu₆₀

amorphous coating/Cu systems were constructed to examine deformation and failure behaviors under nanoindentation using MD simulations. The effects of indenter size on plastic deformation and damage formation were systematically analyzed. These results provide fundamental insights into the deformation mechanisms of Ta–Cu amorphous coatings, contributing to the design of durable, high-performance coating materials.

2. Computational methods

Figure 1(a) illustrates the simulation model of a Ta₄₀Cu₆₀ film deposited on a Cu(001) substrate with dimensions of $18 \times 10.8 \times 8 \text{ nm}^3$ along the X, Y, and Z axes, respectively [12]. The deposition was performed at an incident energy of 1 eV and an incident angle of 0° [14]. The substrate was divided into free, thermostat, and fixed regions. Free atoms followed Newton's law of motion, thermostat layers maintained the target temperature, and fixed layers ensured structural stability. Prior to deposition, energy minimization was conducted to remove high-energy configurations. Simulations were performed mainly under the NVE ensemble with a time step of 0.001 ps, while the NVT ensemble was used when temperature control was required. Periodic boundary conditions were applied along the X and Y directions, and non-periodic conditions along Z. Figure 1(b) shows the nanoindentation

model consisting of a indenter and a $Ta_{40}Cu_{60}$ coating/Cu substrate system ($18 \times 10.8 \times 11.3 \text{ nm}^3$). The diamond tool has diameters of 3, 4, 5, and 6 nm. The embedded atom method (EAM) potential was used for Ta–Ta, Ta–Cu, and Cu–Cu interactions [4], while indenter–substrate interactions were described using the Lennard–Jones (LJ) potential, with parameters $\sigma = 2.86575 \text{ \AA}$, $\varepsilon = 0.13 \text{ eV}$ (C–Ta) and $\sigma = 2.168 \text{ \AA}$, $\varepsilon = 0.05477 \text{ eV}$ (C–Cu).

All molecular dynamics simulations were performed using the LAMMPS package [15], and visualization was conducted using OVITO software [16].

Accordingly, the indentation hardness (H_{iden}) is defined as [11]:

$$H_{\text{iden}} = \frac{F_{\text{Max}}}{A_c} \quad (1)$$

where F_{max} is the maximum force during nanoindentation, and A_c is the contact area between

the $Ta_{40}Cu_{60}$ amorphous coating/Cu substrate and the diamond indenter.

3. Results and discussion

Figure 2(a) presents the indentation force-time curves of $Ta_{40}Cu_{60}$ amorphous coatings on Cu substrates during indentation at a depth of 1.5 nm and a temperature of 300 K under different indenter diameters (3, 4, 5, and 6 nm). The indentation process is divided into three stages: (I) loading, (II) holding, and (III) unloading. In the loading stage (I), the indentation force increases continuously with penetration depth, indicating the accumulation of elastic and plastic deformation in the coating and substrate. During the holding stage (II), a slight decrease in force is observed, which is attributed to the atomic rearrangement and structural relaxation within the amorphous region as the system reaches a quasi-equilibrium state. In the unloading stage

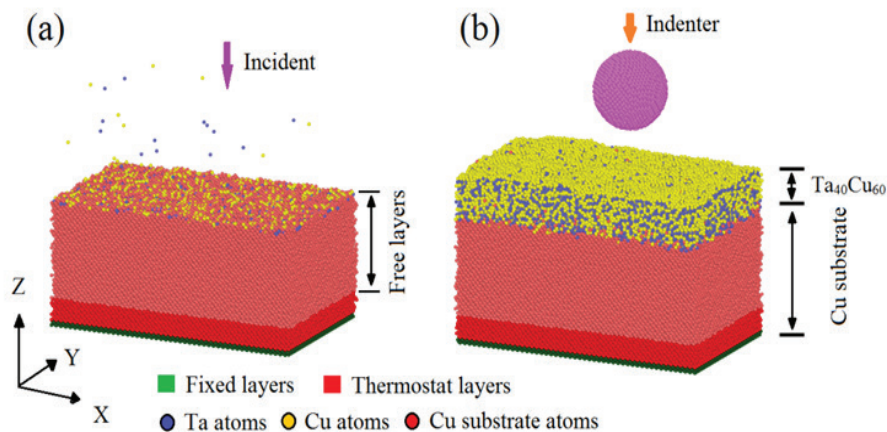


Figure 1. The simulation model is used in the deposition process (a) and nanoindentation process (b).

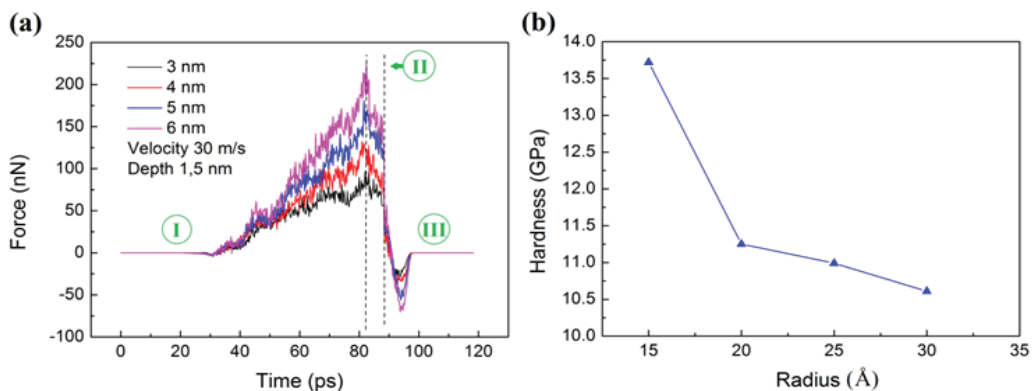


Figure 2. The indentation force (a) and hardness (b) of $Ta_{40}Cu_{60}$ amorphous coatings/ Cu substrate during the indentation process at a depth of 1.5 nm, 300 K under various indenter sizes of 3, 4, 5, and 6 nm.

(III), the force rapidly decreases as the indenter goes up, corresponding to elastic recovery. Interestingly, a small negative force appears at the end of unloading, which originates from adhesive interactions between the indenter and the coating surface. Once the indenter fully detaches, the force returns to zero, confirming the end of contact. The maximum indentation force increases notably with indenter diameter, suggesting that a larger indenter generates a wider contact area and, consequently, a greater load-bearing capacity [15, 17]. However, the hardness, as shown in Figure 2(b), exhibits a decreasing trend with increasing indenter radius. This inverse relationship arises because the hardness calculation involves the applied load divided by the projected contact area larger indenters distribute the load over a broader surface, leading to lower apparent hardness values.

Overall, these findings indicate that indenter size significantly affects both the indentation response and the measured mechanical properties. Larger indenters produce higher peak forces but lower hardness values due to the geometric effect of the contact area and the redistribution of stress beneath the indenter [4].

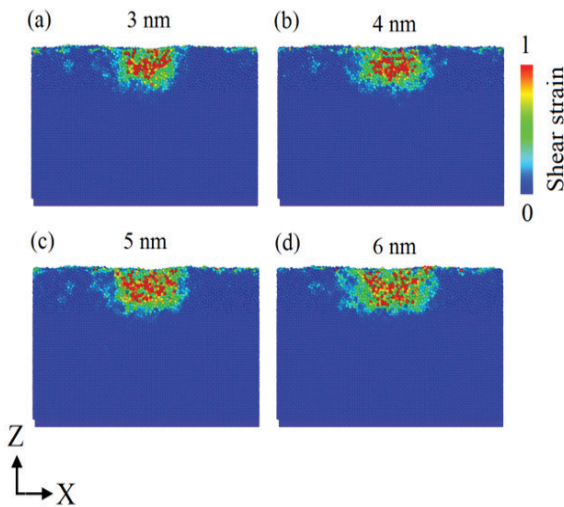


Figure 3. The shear strain of $Ta_{40}Cu_{60}$ amorphous coatings/ Cu substrate during the indentation process under various indenter sizes.

Figure 3(a-d) shows the shear strain distributions in $Ta_{40}Cu_{60}$ amorphous coatings on Cu substrates during nanoindentation using indenters of different diameters (3, 4, 5, and 6 nm). The figure

reveals that the indenter size has a pronounced effect on the extent and morphology of the plastic deformation region. At an indenter diameter of 3 nm, the high-shear-strain zone is localized immediately beneath the contact area, indicating a highly concentrated plastic deformation confined near the surface. As the indenter diameter increases to 4 and 5 nm, the shear strain region becomes more pronounced, expanding both laterally and vertically into the coating and partially into the substrate. This trend suggests that a larger indenter generates a broader stress field, leading to the activation of more shear transformation zones (STZs) and enhanced atomic rearrangements within the amorphous structure [4].

For the largest indenter of 6 nm, the shear strain distribution appears more diffuse and uniform, with a smoother gradient from the high-strain region to the surrounding matrix. This indicates a transition from highly localized deformation toward a more homogeneous plastic flow. The reduction in strain localization with increasing indenter size implies that larger indenters promote distributed deformation, thereby suppressing the formation of dominant shear bands [10]. Overall, these results demonstrate that increasing the indenter diameter not only enlarges the affected deformation volume but also alters the nature of plastic flow in $Ta_{40}Cu_{60}$ amorphous coatings, transitioning from localized shear events to a more uniform deformation behavior.

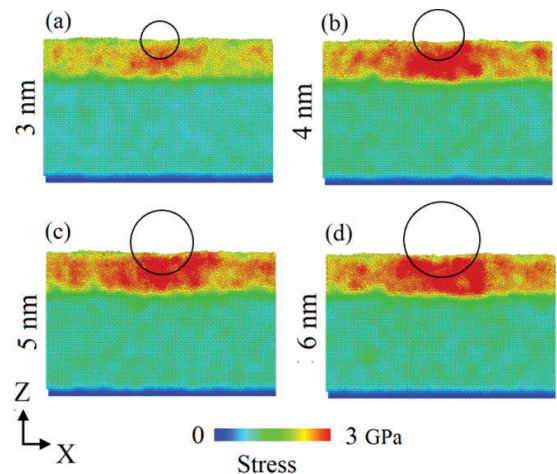


Figure 4(a-d). The local stress of $Ta_{40}Cu_{60}$ amorphous coatings/ Cu substrate during the indentation process under various indenter sizes.

Figure 4(a–d) shows the local stress distribution in the $Ta_{40}Cu_{60}$ amorphous film during nanoindentation with indenter diameters of 3, 4, 5, and 6 nm. The stress magnitude is represented by an atomic color scale ranging from 0 to 3 GPa. It is evident that the $Ta_{40}Cu_{60}$ film exhibits higher stress levels than the Cu substrate, which can be mainly attributed to residual stresses induced during the deposition process. Pronounced high-stress regions are observed at the contact interface between the indenter and the film, consistent with the deformation behavior shown in Figure 3. With increasing indenter diameter, these high-stress zones expand laterally and extend deeper into both the film and the substrate, indicating a more severe deformation response [10,11]. This trend further confirms that larger indenters promote more extensive stress propagation and plastic deformation, in good agreement with the findings reported by Qiu et al. [18] regarding the indenter size effect in metallic thin films.

Figure 5(a–d) illustrates the temperature distribution in the $Ta_{40}Cu_{60}$ amorphous film during nanoindentation with indenter diameters of 3, 4, 5, and 6 nm. The atomic temperature is represented by a color scale ranging from 300 K to 400 K, enabling visualization of localized heat generation during the deformation process.

During indentation, a localized temperature rise occurs directly beneath the indenter tip, resulting from rapid atomic rearrangements associated with plastic deformation. Owing to the absence of long-range order in the $Ta_{40}Cu_{60}$ amorphous structure, shear transformation zones (STZs) are activated under external loading. These STZs act as localized heat sources, leading to the red–yellow regions observed beneath the contact interface between the indenter and the amorphous Ta–Cu film. As the indenter diameter increases from 3 nm to 6 nm, the high-temperature zones expand both laterally and vertically. This behavior indicates that larger indenters induce plastic deformation over a greater material volume. The enlarged deformation region enhances atomic friction and energy dissipation, thereby increasing the local temperature.

Notably, the temperature field within the Cu substrate remains relatively low, suggesting that

most of the generated heat is confined within the amorphous coating rather than being transferred into the crystalline substrate [18]. The spatial correlation between high-temperature regions and high-stress zones (Figure 4) implies a strong coupling between the mechanical and thermal responses. Such coupling is characteristic of metallic glasses, in which localized shear events not only accommodate plastic strain but also serve as primary mechanisms of heat generation.

Overall, these results demonstrate that the thermal response of the $Ta_{40}Cu_{60}$ amorphous film is highly sensitive to indenter size. Larger indenters promote more extensive structural rearrangements, leading to stronger energy dissipation and more pronounced local temperature rises, in agreement with previous studies on metallic glass coatings.

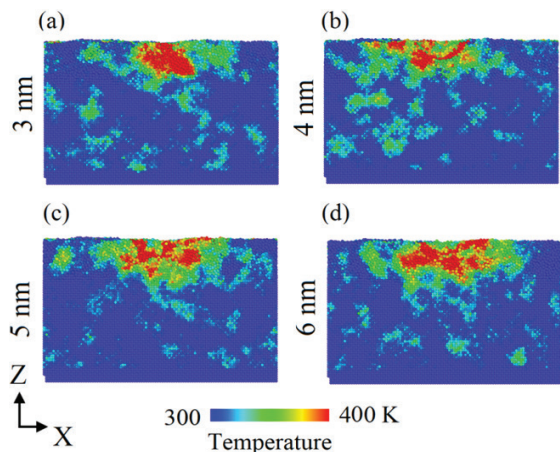


Figure 5(a–d). The Dispersion of temperatures of $Ta_{40}Cu_{60}$ amorphous coatings/ Cu substrate during the indentation process under various indenter sizes.

4. Conclusion

Molecular dynamics simulations were performed to investigate the nanoindentation behavior of $Ta_{40}Cu_{60}$ amorphous coatings on Cu substrates using indenters of various sizes. The results reveal that indenter size has a pronounced influence on the mechanical and thermal responses of the coating. Larger indenters generate higher peak indentation forces but lower hardness values due to the increased contact area. Shear strain analysis indicates that the deformation region expands and becomes more homogeneous with increasing indenter diameter, evolving from localized shear events to more distributed plastic

flow. Correspondingly, high-stress and high-temperature regions develop beneath the indenter and extend deeper into the coating, reflecting enhanced thermomechanical coupling. These findings provide fundamental insights into the size-dependent deformation mechanisms of Ta–Cu amorphous coatings and offer guidance for the design of high-performance metallic glass coatings with improved mechanical stability.

Author Contributions

Conceptualization, P.A.V.; methodology, P.A.V. AND N.T.L.; software, P.A.V AND N.T.L; validation, P.A.V.; writing—original draft preparation, P.A.V AND N.T.L.

Conflicts of Interest

The authors declare no conflicts of interest.

References

- [1] Guo, S. F., Liu, L., & Lin, X., “Formation of magnetic Fe-based bulk metallic glass under low vacuum,” *Journal of alloys and compounds*, vol. 478(1-2), p. 226-228, 2009. <https://doi.org/10.1016/j.jallcom.2008.11.132>.
- [2] Riechers, Birte, et al., “Intermittent cluster dynamics and temporal fractional diffusion in a bulk metallic glass,” *Nature Communications*, vol. 15.1, p. 6595, 2024. <https://doi.org/10.1038/s41467-024-50758-3>.
- [3] Zhao, W., Cheng, J. L., & Li, G., “Quantitative analysis of structure evolution of Zr-Cu amorphous alloys caused by cooling rates based on atomic bond proportion,” *Computational Materials Science*, vol. 186, p. 110011, 2021. <https://doi.org/10.1016/j.commatsci.2020.110011>.
- [4] Song, P., Liu, J., Li, W., & Li, Y., “Plastic deformation behavior of a Cu–10Ta alloy under strong impact loading,” *Defence Technology*, vol. 32, p. 368-382, 2023. <https://doi.org/10.1016/j.dt.2023.02.018>
- [5] Jiang, H., Li, Y., Jiang, L., Zhang, X., Liu, X., Li, L., ... & Lei, Q., “High strength and high conductivity Cu-Ta composites fabricated by powder metallurgy,” *Materials Today Communications*, vol. 38, p. 108183, 2024. <https://doi.org/10.1016/j.mtcomm.2024.108183>.
- [6] Li, N., Chang, Y., Li, M., Chen, Y., Luo, X., Pei, S., & Yang, F., “Enhanced mechanical property by introducing bimodal grains structures in Cu-Ta alloys fabricated by mechanical alloying,” *Journal of Materials Science & Technology*, vol. 172, p. 104-112, 2024. <https://doi.org/10.1016/j.jmst.2023.06.056>.
- [7] Chu, J. P., Jang, J. S. C., Huang, J. C., Chou, H. S., Yang, Y., Ye, J. C., ... & Rullyani, C., “Thin film metallic glasses: Unique properties and potential applications,” *Thin Solid Films*, vol. 520(16), p. 5097-5122, 2012. <https://doi.org/10.1016/j.tsf.2012.03.092>.
- [8] Wu, C. D., & Hou, C. J., “Molecular dynamics analysis of plastic deformation and mechanics of imprinted metallic glass films,” *Computational Materials Science*, vol. 144, p. 248-255, 2018. <https://doi.org/10.1016/j.commatsci.2017.12.042>.
- [9] Apreutesei, M., Esnouf, C., Billard, A., & Steyer, P., “Impact of local nanocrystallization on mechanical properties in the Zr-59 at.% Cu metallic glass thin film,” *Materials & Design*, vol. 108, p. 8-12, 2016. <https://doi.org/10.1016/j.matdes.2016.06.081>.
- [10] Hua, D., Ye, W., Jia, Q., Zhou, Q., Xia, Q., Shi, J., ... & Wang, H., “Molecular dynamics simulation of nanoindentation on amorphous/amorphous nanolaminates,” *Applied Surface Science*, vol. 511, p. 145545, 2020. <https://doi.org/10.1016/j.apsusc.2020.145545>.
- [11] Pham, A. V., Fang, T. H., Nguyen, V. T., & Chen, T. H., “Mechanical response of ZrxCu100-x layer on Cu (001) substrate using molecular dynamics,” *Thin Solid Films*, vol. 737, p. 138954, 2021. <https://doi.org/10.1016/j.tsf.2021.138954>.

- [12] Li, R., Wu, G., Liang, K., Wang, S., Sun, X., Han, X., ... & Liu, S., "Effects of AlN substrate orientation on crystalline quality of wurtzite GaN films investigated via molecular dynamics," *Computational Materials Science*, vol. 202, p. 110991, 2022. <https://doi.org/10.1016/j.commatsci.2021.110991>.
- [13] Mes-adi, H., Herbazi, R., Lablali, M., Saadouni, K., & Mazroui, M., "NiAl (0 0 1) terminated surface effect on the growth of the Al thin film," *Computational Materials Science*, vol. 222, p. 112117, 2023. <https://doi.org/10.1016/j.commatsci.2023.112117>.
- [14] Chocyk, D., & Zientarski, T., "Molecular dynamics simulation of Ni thin films on Cu and Au under nanoindentation," *Vacuum*, vol. 147, p. 24-30, 2018. <https://doi.org/10.1016/j.vacuum.2017.10.008>.
- [15] Ge, G., Rovaris, F., Lanzoni, D., Barbisan, L., Tang, X., Miglio, L., ... & Montalenti, F., "Silicon phase transitions in nanoindentation: Advanced molecular dynamics simulations with machine learning phase recognition," *Acta Materialia*, vol. 263, p. 119465, 2024. <https://doi.org/10.1016/j.actamat.2023.119465>.
- [16] Stukowski, A., "Visualization and analysis of atomistic simulation data with OVITO—the Open Visualization Tool," *Modelling and simulation in materials science and engineering*, vol. 18(1), p. 015012, 2009. DOI 10.1088/0965-0393/18/1/015012.
- [17] Pham, A. V., Chu, V. T., Tran, A. S., Doan, D. Q., Nguyen, V. T., Hoang, V. H., & Vu, H. S., "Deformation behavior and mechanical properties of Ta₄₀Cu₆₀ amorphous coatings by molecular dynamics," *Engineering Research Express*, vol. 7(2), p. 025573, 2025. DOI 10.1088/2631-8695/ade118.
- [18] Qiu, C., Zhu, P., Fang, F., Yuan, D., & Shen, X., "Study of nanoindentation behavior of amorphous alloy using molecular dynamics," *Applied surface science*, vol. 305, p. 101-110, 2014. <https://doi.org/10.1016/j.apsusc.2014.02.179>.

ẢNH HƯỞNG CỦA KÍCH THƯỚC DỤNG CỤ ĐẾN HÀNH VI BIẾN DẠNG CỦA MÀNG MỎNG VÔ ĐỊNH HÌNH Ta-Cu

Tóm tắt:

Mô phỏng động lực học phân tử đã được tiến hành để nghiên cứu hành vi biến dạng của lớp phủ vô định hình Ta₄₀Cu₆₀ trong quá trình tạo vết lõm. Nghiên cứu này cung cấp thông tin chi tiết về ảnh hưởng của kích thước dụng cụ đến cơ chế biến dạng của lớp phủ vô định hình Ta₄₀Cu₆₀/nền Cu. Kết quả cho thấy cả lực ấn cực đại và khu vực biến dạng dẻo của vật liệu đều tăng theo đường kính đầu đo.

Từ khóa: Lớp phủ, Biến dạng, Động lực học phân tử.